Impact of a Revised Convective Triggering Mechanism on CAM2 Model Simulations: Results from Short-Range Weather Forecasts

Shaocheng Xie[1], Minghua Zhang[2], James S. Boyle[1], Richard T. Cederwall[1], Gerald L. Potter[1], and Wuyin Lin[2]

[1]Atmospheric Science Division
Lawrence Livermore National Laboratory

[2]Marine Sciences Research Center
State University of New York at Stony Brook

To be submitted to: Journal of Geophysical Research
Submission Date: 2/24/04
Revised:
Manuscript No:
Receive:

Abstract. This study implements a revised convective triggering condition in the National Center for Atmospheric Research (NCAR) Community Atmosphere Model (CAM2) model to reduce its excessive warm season daytime precipitation over land. The new triggering mechanism introduces a simple dynamic constraint on the initiation of convection that emulates the collective effects of lower level moistening and upward motion of the large-scale circulation. It requires a positive contribution from the large-scale advection of temperature and moisture to the existing positive Convective Available Potential Energy (CAPE) for model convection to start. In contrast, the original convection triggering function in CAM2 assumes that convection is triggered whenever there is positive CAPE, which results in too frequent warm season convection over land arising from strong diurnal variation of solar radiation.

We examine the impact of the new trigger on CAM2 simulations by running the climate model in Numerical Weather Prediction (NWP) mode so that more available observations and high-frequency NWP analysis data can be used to evaluate model performance. The model is initialized with the European Center for Medium-range Weather Forecast (ECMWF) reanalysis (ERA-40). In the study, we show that the modified triggering mechanism has led to considerable improvements in the simulation of precipitation, temperature, moisture, clouds, radiations, surface temperature, and surface sensible and latent heat fluxes when compared to the data collected from the Atmospheric Radiation Measurement (ARM) program at its South Great Plains (SGP) site. Similar improvements are also seen over other parts of the globe. In particular, the surface precipitation simulation has been significantly improved over both the continental United States and around the globe; the overestimation of high clouds in the equatorial tropics has been substantially reduced; and the temperature, moisture, and zonal wind are more realistically simulated.

1. Introduction

Convection over land is overactive during the warm season in the National Center for Atmospheric Research (NCAR) Community Atmosphere Model, (CAM2) and its previous version (CCM3). This has been found both in its single-column model (SCM) simulations [*Xie and Zhang*, 2000; *Ghan et al.*, 2000*; Xie et al.*, 2002; Zhang, 2002], full general circulation model (GCM) short-range weather forecasts [*Boyle et al*., 2004], and climate simulations [*Dai and Trenberth*, 2004]. These studies showed that the model (CAM2 or CCM3) tended to produce convective precipitation almost every day during the summer daytime. They found that this problem is closely related to the convection triggering mechanism used in its deep convection scheme [*Zhang and McFarlane*, 1995] (ZM, hereafter), which assumes that convection is triggered whenever there is positive convective available potential energy (CAPE). The positive CAPE triggering mechanism prevents conditional instability from accumulating in the model before convection begins. As a result, the positive CAPE trigger initiates model convection too often during the day because of the strong diurnal variations in the surface isolation and the induced CAPE diurnal change over land in the warm season.

To illustrate this problem, Figure 1a shows the time series of CAPE (dotted) and surface precipitation (solid) from the observations of the Atmospheric Radiation Measurement (ARM) program [*Stokes and Schwartz*, 1994; *Ackerman and Stokes*, 2003] 1997 Summer Intensive Operational Period (IOP) at its Southern Great Plains (SGP) site. This IOP covers a period from 2330 GMT June 18 to 2330 GMT July 17, 1997. CAPE is calculated from the ARM balloon soundings under the assumption that an air parcel ascends along a reversible moist adiabat with the level of origin at the surface (see Eq. 2.2 in Section 2). It is seen that the ARM SGP site experienced several intensive precipitation events and dry and clear days during this IOP. Most of the convective events occurred in late evening and early morning. Here local noon (standard time) corresponds to 1800 GMT. The observed CAPE, however, exhibits a strong diurnal variation, with maximum during the day and minimum during the night due to the strong solar diurnal cycle over the land surface during the summer. Based on the positive CAPE trigger,

therefore, it is not surprising to see that the CCM3 SCM produced convective precipitation almost every day during the daytime in this IOP (Fig. 1b), where the CCM3 SCM is driven by the large-scale dynamical forcing derived from sounding data collected from this ARM IOP using a constrained variational analysis technique [*Zhang and Lin*, 1997; *Zhang et al*., 2001].

Observations over both midlatitude lands and tropical oceans show that CAPE usually accumulates before convection occurs [e.g., *Zhang and McFarlane*, 1991; *Wang and Randall*, 1994]. The accumulation of large reservoirs of CAPE in nature is a prerequisite for strong convection. To prevent CAPE from being released spontaneously, many efforts have been made in the past to link convective trigger to the large-scale dynamic processes (e.g., large-scale low-level convergence) since these processes play a key role in destabilizing the atmospheric structure and initiating deep cumulus convection. For example, *Kuo* [1965, 1974] linked the convective trigger with the large-scale moisture convergence in his convection scheme. *Fritsch and Chappell* [1980], *Kain and Fritsch* [1993], and *Rogers and Fritsch* [1996] parameterized perturbations of temperature and vertical velocity based on the large-scale low-level convergence to help avoid excessive convection in areas where the low-level upward motion is weak. To reduce the problem associated with the convective triggering mechanism in the ZM scheme, *Xie and Zhang* [2000] introduced an empirical dynamic constraint after experimenting with a variety of potential large-scale control variables. A dynamic CAPE generation rate (DCAPE) determined by the large-scale advective tendencies of both the temperature and moisture is used to control the onset of deep convection. In their study, DCAPE is defined as the change of CAPE solely due to the total large-scale advection over a time interval (see Eq. 2.1 in Section 2). They assumed that deep convection occurs only when the large-scale advection makes a positive contribution to the existing positive CAPE. This large-scale dynamic constraint allows CAPE to accumulate from surface processes before convection occurs and it also links model deep convection closely to the large-scale dynamical processes, including large-scale upward motion and low-level moisture convergence. *Xie* [1998] showed a strong in-phase correlation between positive DCAPE and convective activities using data collected over both midlatitude land and tropical ocean. This relationship is also shown in this 1997 Summer ARM IOP data (Fig. 1c).

Using the CCM3 SCM, *Xie and Zhang* [2000] showed that the dynamic constraint could largely reduce the effect of the strong diurnal variation in the surface insolation on the initiation of convection and considerable improvements can be obtained in the model simulation of precipitation field when the dynamic constraint was applied to the model triggering function (Fig. 1d). However, the performance of the improved convection triggering mechanism in the full GCM has not been tested.

We recently implemented the convection triggering mechanism proposed by *Xie and Zhang* [2000] into the CAM2 model and evaluated its impact on CAM2 simulations in both short-range weather forecasts and climate simulations. The short-range weather forecasts are conducted under the U.S. Department of Energy (DOE)'s Climate Change Prediction Program (CCPP) - ARM Parameterization Testbed (CAPT) framework [*Phillips et al*., 2004], which provides a flexible environment for running climate models in Numerical Weather Prediction (NWP) mode. In comparison with testing physical parameterizations in climate simulations, the CAPT strategy uses more available observations and high-frequency NWP analyses to evaluate model performance in short-range weather forecasts. This allows specific parameterization deficiencies to be identified before the compensation of multiple errors masks the deficiencies, as can occur in model climate simulation. Another advantage of the CAPT approach is its capability to link model deficiencies directly with atmospheric processes through case studies using data collected from major field programs (e.g., ARM). In this paper, we will focus on evaluating model performance from the CAPT framework. Impact of the new triggering mechanism on climate simulations will be reported in a separate study.

This paper is organized as follows. Section 2 briefly describes CAM2 and model initialization procedures. Section 3 discusses comparison strategy and evaluation data. Comparison of model results with the ARM observations during the 1997 Summer IOP at the ARM SGP site is discussed in Section 4. Section 5 provides regional and global views on the model performance by comparing with satellite measurements and NWP reanalysis data. Results are summarized in Section 6.

2. CAM2 and model initialization procedures

The model used in this study is the NCAR Community Atmosphere Model (CAM2), which is the fifth generation of the NCAR atmospheric GCM. It is a global spectral model with T42 truncation (2.8^0 x 2.8^0, which is around 300 km) in the horizontal and 26 levels in the vertical. Compared to its earlier version CCM3 [*Kiehl et al*., 1998], CAM2 incorporates significant improvements to its physical parameterizations, including generalized cloud overlap for radiation calculation, a new parameterization for longwave absorptivity and emissivity of water vapor, a prognostic scheme for cloud condensed water, a new sea-ice formulation, an explicit representation of fractional land and sea-ice coverage, and evaporation of convective precipitation. CAM2 retains the same deep convection scheme (the ZM scheme) as used in CCM3. The ZM scheme is based on the plume ensemble concept similar to *Arakawa and Schubert* [1974]. Shallow convection is represented using the scheme developed by *Hack* [1994]. More detailed information about CAM2 can be seen in *Collins et al*. [2003].

As discussed earlier, the ZM scheme assumes that convection occurs whenever there is a positive CAPE. In reality, convection is triggered when an air parcel or a subgrid scale cell is energetic enough to penetrate the layer of convection inhibition. This penetration is typically associated with one of the following scenarios: large-scale upward motion associated with synoptic scale systems, existing convection, subgrid scale dynamic instability, surface heterogeneity, or growth of the boundary layer. After experimenting different control variables observed at the ARM SGP site, *Xie and Zhang* [2000] (XZ trigger, hereafter) found that the large-scale dynamic condition had the dominant control on the occurrence of convection, and that the combined measure of lifting and inhibition was empirically described by the positive contribution of large-scale advection to CAPE, including upward motion and lower-level moistening by the grid-scale circulation. We implement this triggering function in the CAM2 model. It requires that deep convection occurs only when the large-scale advective tendencies of temperature and moisture make a positive contribution to the existing positive CAPE, i.e., DCAPE > 0 and CAPE > 0. DCAPE is defined as:

$$DCAPE = (CAPE\ (T^*, q^*) - CAPE\ (T, q))/\Delta t \qquad (2.1)$$

where (T, q) are the temperature and specific humidity in the current atmospheric state and (T^*, q^*) are (T, q) plus the change due to the total large-scale advection over a time interval Δt. CAPE is calculated under the assumption that an air parcel ascends along a reversible moist adiabat.

$$CAPE = R_d \int_{Pi}^{Pn} (T_{vp} - T_v) d\ln p \qquad (2.2)$$

where Pn is the neutral buoyancy pressure for an air parcel originating from Pi. T_{vp} is the virtual temperature of the parcel, and T_v is the virtual temperature of the ambient air at the same level.

As part of the CAPT framework, the CAM2 model is initialized with the European Center for Medium-range Weather Forecast (ECMWF) reanalysis [ERA-40, *ECMWF*, 2002]. The ERA-40 reanalysis data were generated every 6 hours by implementing a three-dimensional variational analysis technique that uses the T159L60 version of the ECMWF Integrated Forecasting System. In our implementation, the finer-resolution reanalysis data were mapped to the coarser CAM2 resolution. Initial values for the prognostic parameterized variables (e.g., cloud water) are obtained via a spin-up procedure that is described in *Phillips et al*. [2004] in conjunction with the land initialization.

To examine the quality of the initial data, Figure 2 gives the root-mean-square (RMS) errors (solid lines) of the atmospheric state variables from the ERA-40 reanalysis averaged over the ARM SGP domain for the 1997 Summer IOP. The standard deviations of the ARM observed fields (dashed lines) are also shown in the figure to show the size of the RMS error relative to the variability in the observed field itself. The RMS error in the ERA-40 reanalysis is typically less than 1.5 m s^{-1} in the horizontal winds within most of the troposphere except the levels above 315 hpa where the RMS error is slightly larger. The temperature field shows the RMS error around

0.5 K in the mid- and lower troposphere between 865 hpa and 465 hpa and less than 1 K for the entire troposphere from 915 hpa to 215 hpa. Near the surface and above 215 hpa, the temperature error is quite large. The RMS error in the moisture field decreases with height. It is less than or around 1 g kg^{-1} in most of the troposphere except for the lowest level where the RMS error is about 1.5 g kg^{-1}. These errors may in part occur because the ARM sounding measurements were not used in the ERA-40 data assimilation system. The rather large errors shown in horizontal winds and temperature in the upper troposphere may be also due to relatively large uncertainties in the ARM sounding measurements at those levels. In comparison with the observed standard deviations (dashed lines), the RMS errors are considerably smaller than the observed temporal variability itself.

3. Comparison strategy and evaluation data

To evaluate model physical parameterizations, a series of short-range forecasts (24 hours) were conducted under the CAPT framework in order to ensure that the model produced large-scale circulation has not been drifted away from observations. These runs were initiated every day at 00Z for 30 days starting from 18 June 1997 to 17 July 1997 to cover the ARM 1997 Summer IOP. Selected meteorological fields are discussed with a focus on the model-simulated precipitation and other associated fields. Comparisons are made with both field measurements and global satellite data and NWP reanalyses.

The field measurements are from the data collected from the ARM SGP site during its 1997 Summer IOP, which contained a wide range of summertime midlatitude weather conditions. The ARM program is a key part of the DOE effort to address scientific uncertainties in global climate changes with a specific focus on improving the performance of current climate models for climate research and prediction. To reach this goal, the ARM program has conducted a number of extensive field campaigns to collect data for evaluation and improvement of model physical parameterizations, especially radiation and cloud parameterizations. During the ARM IOPs, sounding balloons at five sounding stations (* in Fig. 3) are launched every three-hours to

measure the vertical profiles of temperature, water vapor mixing ratio, and winds. There are also 7 NOAA wind profiler stations near the SGP site (◇ in Fig. 3) taking hourly winds. Within the SGP domain (circled by the variational analysis grids • in Fig. 3), there is a dense surface measurement network, which was described in *Zhang et al*. [2001], along with satellite measurements from the Geostationary Operational Environment Satellite (GOES). These platforms include the Surface Meteorological Observation Stations (SMOS) and the Oklahoma and Kansas mesonet (OKM and KAM) stations that measure surface precipitation, pressure, winds, temperature and relative humidity; the Energy Budget Bowen Ratio (EBBR) stations and the Eddy Correlation Flux Measurement System (ECOR) that measure surface latent and sensible heat fluxes and surface broadband net radiative flux; the microwave radiometer (MWR) stations that measure the column precipitable water and total cloud liquid water; and the surface Solar Infrareed Radiation Stations (SIRS) that provide 1 minute continuous measurements of broadband shortwave and longwave irradiances for downwelling and upwelling components. The hourly Arkansa Basin Red River Forecast Center (ABRFC) 4-km rain gauge adjusted WSR-88D radar measurements over the domain are also available and provide the best estimate of the spatial distribution of precipitation. The satellite measurements of clouds and broadband radiative fluxes are available from the 0.5 x 0.5 degree analysis of the GOES data [*Minnis et al*., 1995].

To make comparisons more meaningful between model outputs and the ARM observations, the SGP domain-averaged ARM data are needed. The domain-averaged atmospheric state variables are obtained from merging the sounding and wind profiler data through the constrained objective variational analysis [*Zhang and Lin*, 1997; *Zhang et al*., 2001]. In order to avoid biases of using overcrowding measurement stations in some areas, the domain-averaged surface variables are obtained by first laying the 0.5^0 x 0.5^0 GOES grids over the SGP domain, and then deriving the required quantities in each small grid box. If there are actual measurements within the subgrid box, simple arithmetic averaging is used to obtain the subgrid means. Some variables are available from several instruments as discussed earlier. They are merged in the arithmetic averaging process. If there is no actual measurement available in the

small box, the Barnes scheme [*Barnes*, 1964] is used to fill the missing data. Domain averages of these quantities are obtained by using values from the 0.5^0 x 0.5^0 grid boxes within the analysis domain. More details can be seen in *Zhang et al*. [2001].

Since the CAM2 grid box does not match the SGP domain exactly as shown in Fig. 3 that gives four surrounding model grid boxes (the four small squares A, B, C, and D centered by the model grid points ×) at the ARM SGP site, model outputs are averaged over the four model grid boxes using weights proportional to the overlap area of the CAM2 grid box with the ARM SGP domain when compared with the ARM observations. Therefore, model results actually represent averages over a domain that is slightly larger than the ARM SGP domain. This should be borne in mind in the following discussions.

In order to evaluate model results in the areas beyond the ARM SGP site, we compare the model-produced precipitation with the observations taken from Global Precipitation Climatology Project (GPCP) daily 1^0 x 1^0 gridded precipitation data [*Huffman et al*., 2001]. The GPCP precipitation data are obtained by merging satellite estimates of precipitation with rain gauge data from surface-based stations. The model clouds are evaluated against the measurements from International Satellite Cloud Climatology Project (ISCCP) D1 3-hourly cloud products [*Rossow et al*. 1996]. ISCCP cloud products classify cloud types based on their top pressure and optical thickness. To facilitate the evaluation, an ISCCP simulator [*Klein and Jacob*, 1999 ; *Webb et al*. 2001] is added as a run-time diagnostic package in CAM2 to emulate the ISCCP algorithm. The ISCCP simulator diagnoses model clouds in a similar way that a satellite would view an atmosphere with physical properties (e.g., cloud height, cloud cover, and optical depth) specified by the model. *Lin and Zhang* [2004] described the details of implementing the ISCCP simulator in CAM2. For the atmospheric state variables, we compare the model simulations with the ERA-40 reanalyses.

4. Comparison with the ARM measurements at the SGP site

4.1. Time series of precipitation, clouds, and surface temperature

We first examine the model-produced surface precipitation rates since they are closely associated with model cumulus convection scheme. For convenience, we use CAM2O to represent the original model and CAM2M to represent the model with the modified triggering mechanism, and OBS to represent observations in the following discussions. Figure 4 shows the time series of surface precipitation rates for CAM2O, CAM2M, and the corresponding observations averaged over the ARM SGP domain. The model result is 0 to 24 hour forecasts from a series of 24-hour runs concatenated for the ARM 1997 Summer IOP. We use the same method to construct other fields that we will discuss later. As we discussed earlier, during this IOP, the ARM SGP site experienced several intensive precipitation events and dry and clear days. Most of the heavy precipitation events are associated with a complex of thunderstorms that developed outside the ARM SGP domain in the late evening and moved across the ARM SGP domain (e.g., the precipitation events on days 8, 11-12, and 21). Here "day n" refers to the day between n-1 and n in the plots. This convention is used throughout the paper. Some precipitation events are associated with localized individual thunderstorms (e.g., the weak precipitation event on day 10, the moderate precipitation events on days 22-23). Most of the convective events are dominated by cumulus precipitation [*Xie et al*., 2002]. The dry and clear periods are associated with strong large-scale downward motions.

It is seen that the original CAM2 largely overestimates the frequency of the observed precipitation occurrence. It tends to produce precipitation almost everyday (Fig. 4a), similar to the results seen in the CCM3 SCM test (Fig. 1b). This problem is noticeably reduced in CAM2M when the XZ trigger is used (Fig. 4b). The dynamic constraint introduced in the XZ trigger effectively prevents convection from being fired every day in the model. It is noticed that both models largely underestimate the observed precipitation during strong convective periods. This is not uncommon in climate models, which typically use horizontal resolutions that are larger than 200 km, in simulating these subgrid-scale dominated convective processes. The problem could be reduced with increasing the model resolutions [*Duffy et al*., 2003]. In addition, as we discussed before, the model precipitation is averaged over an area that is slightly larger

than the ARM SGP domain. This could also contribute to the weak magnitude of the events produced in the models.

Clouds are another field that is largely affected by model cumulus parameterizations. Figures 5a, b compare the high cloud fraction produced by CAM2O and CAM2M to the GOES satellite observations, respectively. CAM2O shows much larger temporal variability in its produced high clouds in comparison with the GOES high clouds. This is clearly related to the too frequent convection produced in this model. The observed high clouds are overestimated by CAM2O, especially during non-precipitation periods (e.g., on days 1-4 and days 13-15). In contrast, the observed temporal variability is well reproduced in CAM2M and the overestimation of high clouds in CAM2O is significantly reduced in CAM2M during non-precipitation periods because of less convection produced with the improved convective trigger. Similar improvements can be seen in the outgoing long-wave radiative flux (OLR, not shown), consistent with the improvements in the high clouds.

The observed and model simulated surface temperature fields are shown in Fig. 6. The observations (solid line) show very strong diurnal variations. This feature is well captured by both models. However, the surface temperature in CAM2O is too cold compared to the observations (Fig. 6a). One of the reasons is because convection is too active in CAM2O, which results in excessive clouds, and then leading to less solar radiation reaching the surface. With the new triggering scheme, the excessive clouds are largely reduced. This results in large improvements in the surface temperature simulation, which is in a better agreement with the observations (Fig. 6b).

4.2. Simulations of temperature and moisture fields

The temporal evolution of the ARM observed temperature and differences between the simulated temperature and the observed value over the SGP domain are shown in Fig. 7. The original model (CAM2O) shows a systematic warm bias in most troposphere, especially in the mid- and upper troposphere between 565 hpa and 215 hpa, when compared to the ARM observations (Fig. 7b). The warm bias is clearly related to the model-produced overactive

convection that releases excessive convective heating at these levels. While this error is also shown in CAM2M, it has been considerably reduced (Fig. 7c). The largest improvement is between 565 hpa and 215 hpa. Beyond these levels, both CAM2O and CAM2M display a very similar error pattern with a comparable magnitude of the model bias. Both models become too cold in the level above 215 hpa. This is probably related to the error in the initial data. As shown in Fig. 9a, the initial data show a rather large cold bias above 215 hpa compared to the ARM data.

Figure 8 is the same as Fig. 7 except for the moisture simulation. Both CAM2O and CAM2M (Figs. 8b,c) show a systematic dry bias in the mid-and lower troposphere over the entire period except for days 16-18, where both models produce a significant moist bias due to the failure to capture the abrupt reduction of moisture shown in the observations during that period (Fig. 8a). However, the magnitude of the dry bias in CAM2M is smaller than that in CAM2O because convection is less active in CAM2M than the original model. This results in less moisture consumed by convection in CAM2M.

The vertical distributions of temperature and moisture errors (compared to the ARM data) averaged over the 30 days are shown in Figs. 9a and 9b, respectively. For better understanding of these errors, the mean errors in the initial data are also shown in the figures (dotted lines). It is seen that the initial data show a warm bias of less than 0.5 K in the mid- and lower troposphere between 865 hpa and 515 hpa. The warm bias increases with height and reaches a maximum of around 1 K at 265 hpa. The initial data show a cold bias in the boundary layer below 865 hpa and a rather large cold bias above 215 hpa. The difference between the initial data and the ARM observations in the moisture field is quite small in the levels above 815 hpa. Below this level, the initial data show a dry bias of less than 1 g kg^{-1}. Even considering the potential errors in the initial data, CAM2O still shows a quite large warm bias in the mid- and upper troposphere between 865 hpa and 215 hpa and a large cold bias below 865 hpa in its 24-hour forecasts. For moisture, CAM2O has a quite large dry bias below 515 hpa and a small moist bias above. These errors are considerably reduced in CAM2M. The magnitude of the model errors in CAM2M is comparable to that in the initial data. As we mentioned earlier, the large cold biases produced

by both CAM2O and CAM2M in the upper troposphere are probably due to the large cold bias in the initial data.

4.3. Mean surface energy budgets

Table 1 presents the time-averaged surface energy budget components for CAM2O, CAM2M, and the ARM observations over the entire IOP at the SGP site. In the table, SWS and LWS are net surface shortwave and longwave radiative fluxes, respectively. LH is surface latent heat flux and SH is surface sensible heat flux. The observed surface radiative fluxes are from the ARM surface Solar Infrared Radiation Stations measurements. The ARM EBBR and ECOR instruments provide the observed surface latent and sensible heat flux data.

Table 1. The mean surface energy budgets (W m^{-2}) averaged over the ARM 1997 Summer IOP for the SGP site.

Field	Observation	CAM2O	CAM2M
SWS	227.483	203.944	221.878
LWS	63.409	55.938	63.979
LH	113.640	146.049	131.583
SH	36.279	10.714	27.435
Net surface	14.567	-8.757	-1.119

It is seen from the table that the simulated surface net shortwave and longwave radiative fluxes in CAM2O are smaller than observed by -23.5 W m^{-2} for shortwave radiation and -7.5 W m^{-2} for longwave radiation, respectively. CAM2O simulated sensible heat flux is 25.6 W m^{-2} less than the ARM observations, which is consistent with the colder surface produced in the model (Fig. 6a), and latent heat flux is 32.4 W m^{-2} larger than the observed. For these surface energy budget terms, CAM2M shows much better agreement with the observations than CAM2O. The differences between CAM2M and the observations are within 6 W m^{-2} in

shortwave radiation, 0.5 W m^{-2} in longwave radiation, 8.8 W m^{-2} in sensible heat flux, and 17.9 in latent heat flux, respectively. The net surface energy budget in CAM2M is also much closer to the observed value than CAM2O. This is consistent with the more realistic surface temperature produced in CAM2M (Fig. 6b).

The above discussions have shown that the XZ trigger improves overall the CAM2 simulations in the short-range weather forecasts when compared to the ARM field measurements. The improvements are similar to those obtained in the SCM tests [e.g., *Xie and Zhang*, 2000]. However, it should be noted that improvements made in SCM tests are not guaranteed to be transferable to its parent GCM due to the limitation of the SCM framework, such as the lack of the internal feedback between the model dynamical processes and physical processes. The encouraging results shown in this study indicate that the improved scheme proposed by *Xie and Zhang* [2000] based on the SCM framework has passed the test in a full GCM, at least for the same geographical location (the SGP site).

5. Regional and global simulations

5.1. Precipitation

To examine the impact of convective trigger on simulations in regions beyond the ARM SGP site, Figure 10 displays the geographical distribution of precipitation over the region that covers the continental United States. The model data are 0-24 hour forecasts averaged over the 30 days as described earlier. The observations are taken from Global Precipitation Climatology Project (GPCP) daily precipitation data [*Huffman et al*., 2001] and these data are averaged over the same period as that covered by the model data. During the summer period, the heaviest precipitation is seen in the southeast and along the Gulf Coast in the GPCP data (Fig. 10c). Another relatively large rainfall region in the observations is located southwest of the Great Lakes along the Mississippi-Wisconsin Rivers. Light precipitation is seen between these two major precipitation areas from the southwestern U.S. stretching northeastward into the Northeast Coast. Overall, the observed spatial pattern of precipitation appears to be more realistically

simulated in CAM2M than CAM2O (Fig. 10a and 10b). The locations of the two maximum precipitation centers in the southeast and along the Gulf Coast in the observations are well captured by CAM2M. Another observed large precipitation region along the Mississippi-Wisconsin rivers is also reasonably reproduced in CAM2M, although the area of the modeled precipitation is larger than the observations. In contrast, the original model CAM2O overestimates the observed precipitation in most parts of the country. It is noticed that CAM2O shows a precipitation maximum located to the east of the Rockies, which is not shown in the observations. This phenomenon is also present in the summer precipitation field for the mean of all CMIP (Coupled Model Intercomparison Project) models [*Coquard et al*., 2003]. Results from our study indicate that the CMIP model systematic error can be detected in the early stage of model integration. This has important implications for understanding what model deficiencies cause the systematic error since it allows us to perform a more in-depth analysis during a short time period where more observations are available and different model errors from various processes have not compensated for the systematic error. It is interesting to see that this bias is largely reduced in CAM2M, indicating that problems associated with model cumulus parameterization should partly account for this systematic climate error.

In addition to these improvements over the midlatitude lands, CAM2M also shows very encouraging results in other areas, including the tropical and subtropical regions as shown in Fig. 11, which gives the global distribution of precipitation for CAM2O, CAM2M, and the observations. It is seen from Fig. 11b that CAM2M reproduces well the principal features of the observed precipitation distribution, particularly in the Tropical Pacific and India Oceans and in North Africa. In contrast, CAM2O produces excessive precipitation over a broader region in comparison with the observations but it underestimates the magnitude of the observed precipitation maxima, such as those in the eastern Pacific and in the northeastern boundary of the Bay of Bengal (Fig. 11a). These results indicate the triggering mechanism developed by *Xie and Zhang* [2000] based on the midlatitude observations is suitable for use globally.

5.2. Clouds

The global distribution of high clouds from CAM2O, CAM2M, and the ISCCP satellite measurements is shown in Fig. 12. As discussed earlier, the model clouds are diagnosed by using the ISCCP simulator with cloud physical properties specified from the CAM2 model. Since ISCCP clouds are not available during nighttime, only daytime model clouds from the series of 0-24 hour forecasts are averaged over the 30 days. During the summer period, the ISCCP clouds (Fig. 12c) show a maximum band of clouds along the equatorial Pacific in the vicinity of Intertropical Convergence Zone (ITCZ), the Southern Asia continents, and Indian Oceans and two minimum bands of clouds in the subtropical regions associated with the strong downward branch of the Hadley circulation. In general, both models capture this spatial pattern of the ISCCP high clouds. However, CAM2O substantially overestimates the high cloud amount in tropics and underestimates the high clouds in the subtropics. Note that these biases are also shown in its climate simulations [*Lin and Zhang*, 2004], indicating that the systematical errors in both climate simulation and weather forecasts could be due to the same deficiencies in the model. In contrast, CAM2M reproduces the observed high clouds remarkably well in the tropics even though it also underestimates the subtropical high clouds as shown in CAM2O. The improvements in the high clouds are consistent with the improvements in the simulated precipitation in the tropical regions as shown in Fig. 11. The result suggests that the systematic overestimation of the observed high clouds in the tropics in CAM2 may be largely related to problems associated with its deep convection scheme rather than its cloud scheme.

5.3. Temperature, moisture, and zonal wind

The model-produced zonally averaged mean temperature, moisture, and zonal wind from the series of 24-hour forecasts over the 30 days are compared with the ERA-40 reanalysis data. Figures 13a-c respectively give the zonally averaged mean temperature from the ERA-40 reanalyses and the differences between the models and the reanalysis data. In comparison with the reanalysis data, both models produce very similar errors in the lower and upper troposphere, such as the quite large warm biases in the mid- and high latitudes in both hemispheres below 800 hpa. Between 600 hpa and 200 hpa, the temperature error produced by CAM2O and CAM2M is quite different, especially in the tropical and subtropical regions from 30N to 30S, where CAM2O shows a rather large warm bias of up to 1 K while CAM2M just produces a small cold

bias (less than –0.5 K). The warm bias in CAM2O is likely related to its overestimation of convection in these regions as indicated in its precipitation field (Fig. 11a). In general, CAM2M produces a colder atmosphere with smaller errors than CAM2O in the mid-troposphere because of less convection triggered in the model.

Similar results are also seen in the zonally averaged mean moisture field (Figs. 14a-c). Compared to the ERA-40 reanalyses, the model error in moisture field is small in the mid- and high latitudes because of less moisture in these regions than in the tropical and subtropical regions (Fig. 14a). Between 30N and 30S, CAM2O produces a large dry bias in the lower troposphere (Fig. 14b), which is consistent with the large warm bias shown in the mid- and upper troposphere in its temperature simulation (Fig. 13b). Again, this indicates that convection in CAM2O is too active, which results in excessive moisture consumed in the lower troposphere and excessive convective heating released in the mid- and upper troposphere. With the new convective trigger, CAM2M dramatically reduces this dry bias (Fig. 14c). It is also noted that both models show a relatively large moist bias near the surface. This may reflect problems associated with model boundary layer processes, which are not able to effectively transport moisture from surface to upper troposphere. As shown in Boyle et al. (2004), the boundary height produced by the CAM2 model is too low compared to the ARM measurements at the SGP site.

The zonal wind is another important field that people usually use for verification of model simulation. During the summer season, the ERA-40 reanalysis data show a strong westerly maximum at 200 hpa near 40N over North Hemisphere and a stronger westerly maximum at 200 hpa near 30S over Southern Hemisphere (Fig. 15a). In the tropical regions, the ERA-40 reanalyses show weak easterlies. Overall, the zonal wind structure is well simulated by both models. However, the zonally averaged westerlies in CAM2O are much stronger than the reanalysis data in the upper troposphere between 30N and 40N and between 10S and 30S (Fig. 15b). This is probably related to the increased meridional temperature gradients in the mid- and upper troposphere in CAM2O due to the large warm bias produced in its simulated temperature field in the tropics and subtropics. Larger meridional temperature gradients lead to stronger westerlies. These westerly biases are significantly reduced in CAM2M, consistent with its improved temperature field (Fig. 15c). It is also noted that the rather large westerly bias near

10N and easterly bias near 10S in the lower troposphere in CAM2O are also slightly reduced in CAM2M.

6. Summary and discussions

In this study, we implemented the convective triggering mechanism proposed by *Xie and Zhang* [2000] in CAM2 in order to reduce the too frequent convection in the original model during warm season over land. The performance of the CAM2 with the modified convective triggering mechanism was evaluated under the CAPT framework, in which the climate model is run in NWP mode with the initial data obtained from the ERA-40 reanalysis. A series of 24-hour forecasts were conducted by initiating the model every day at 00Z for 30 days from 18 June 1997 to 17 July 1997. Model results are compared with the observations collected from the ARM 1997 Summer IOP at the SGP site, the global GPCP precipitation data and ISCCP satellite cloud data, and the ERA-40 reanalyses. At the ARM SGP site, we have shown that CAM2M significantly reduces the frequency of model convection when compared to CAM2O, generally in a better agreement with the ARM observations. This results in a more realistic simulation of other important atmospheric fields, such as temperature, moisture, clouds, radiation, surface temperature, and surface sensible and latent heat fluxes. When compared to CAM2O, for example, CAM2M showed a much smaller warm/dry bias in its simulated temperature and moisture fields; the overestimation of high clouds and underestimation of surface temperature were substantially reduced; and surface energy budgets are closer to the ARM observations.

The distributions over the continental US and the globe of the simulated precipitation and high clouds in CAM2M showed an excellent agreement with the observations. The principal features of the observed precipitation and tropical high clouds were dramatically reproduced, both in spatial pattern and magnitude. In contrast, CAM2O generally overestimates these fields mainly due to the overestimation of the frequency of convection occurrence.

The zonally averaged mean temperature is generally colder in the troposphere in CAM2M than CAM2O due to less convection triggered in CAM2M. Significant improvements have been shown in the mid- and upper troposphere between 30N and 10S, where the large warm bias in CAM2O is greatly reduced. Consistent with the improvements in the temperature, CAM2M substantially reduced this large dry bias in the lower troposphere between 30N and 10S

in CAM2O. In addition, the westerlies in the upper troposphere between 30N and 40N and between 10S and 30S are also improved in CAM2M.

It is interesting to note that the biases shown here in the CAM2 short-range weather forecasts are also the systematic errors in the CAM2 climate simulations. Examples are the extremely overestimated high clouds in the tropics in the vicinity of ITCZ and the spurious precipitation maximum in the east of the Rockies. This suggests that the systematical errors in both climate simulation and weather forecasts could be due to same reasons. Thus, running the climate model in NWP mode can help us to identify what model deficiencies cause the systematic climate errors. The reduction of these errors in CAM2M shown in this study suggests a potential link between the climate errors and problems associated with model cumulus parameterizations.

This study represents an example of how to efficiently transfer improved parameterizations made from SCM tests to 3-dimensional climate models before they can be used to improve climate simulations. It has shown that the modified trigger is suitable to use globally. Evaluation of the new triggering mechanism in climate simulations is currently underway. Preliminary results from a ten-year climate simulation using CAM2M show a number of desirable improvements in the simulation of surface precipitation, clouds, and other fields, particularly over tropical and sub-tropical regions, when compared to CAM2O. Some systematic climate errors, such as the unrealistic double Intertropical Precipitation Zone (ITPZ) and the excessive high clouds produced in CAM2O, are noticeably reduced. Details about the climate simulations will be reported as part of a separate study.

Acknowledgements. This research was performed under the auspices of the U. S. Department of Energy (DOE) Office of Science, Biological and Environmental Research by the University of California, Lawrence Livermore National Laboratory under contract No. W-7405-Eng-48. Work at SUNY Stony Brook was supported by ARM grant DE-FG02-98ER62570 and was also supported by NSF under grant ATM9701950. The ARM Data were obtained from the Atmospheric Radiation Measurement (ARM) Program supported by the DOE office of science. We would like to thank Dr. James Hack from NCAR for several useful discussions on the revised convective triggering function. We thank John Yio for his great help on processing the

ARM data. Support from the LLNL CAPT team is greatly appreciated. The Climate Data Analysis Tools (CDAT) that were developed in the Program for Climate Model Diagnosis and Intercomparison (PCMDI) were used to perform our analyses.

References

Arakawa, A., and W. H. Schubert, Interaction of a cumulus cloud ensemble with the large-scale environment, Part I, *J. Atmos. Sci*., *31*, 674-701, 1974.

Ackerman, T.P., and G.M. Stokes, The Atmospheric Radiation Measurement Program. *Physics Today*, 56, 38-44, 2003.

Barnes, S. L., A technique for maximizing details in numerical map analysis. *J. Appl. Meteor*., 3, 396-409, 1964.

Boyle, J. S., and coauthors, Diagnosis of CAM2 in NWP configuration, *In preparation for submission to J. Climate*, 2004.

Collins, W. D., and coauthors, Description of the NCAR Community Atmosphere Model (CAM2), 171 pp., 2003. [Available online from http://www.ccsm.ucar.edu/models/atm-cam/docs/]

Coquard, J., and coauthors, Simulations of western U. S. surface climate in 15 global climate models, *submitted to Climate Dynamics*, 2004.

Dai, A. and K. T. Trenberth, The diurnal cycle and its depiction in the Community Climate System Model, *J. Climate, In press*, 2003.

Duffy, P. B., and coauthors, High resolution simulations of global climate, Part 1: present climate, *Climate Dynamics, 21*, 371-390, 2003.

ECMWF, ECMWF re-analysis ERA, 2002. [Accessible online at http://www.ecmwf.int/research/era]

Fritsch, J. M., and C. F. Chappell, Numerical prediction of convectively driven mesoscale pressure systems, Part I: Convective parameterization, *J. Atmos. Sci., 37*, 1722-1733, 1980.

Ghan, S. J., and coauthors, An intercomparison of single column model simulations of summertime midlatitude continental convection, *J. Geophys. Res., 105*, 2091-2124, 2000.

Hack J. J., Parameterization of moist convection in the National Center for Atmopsheric Research Community Climate (CCM2), *J. Geophys. Res., 99*, 5551-5568, 1994.

Huffman, G.J., and coauthors, Global Precipitation at One-Degree Daily Resolution from Multi-Satellite Observations, *J. Hydrometeor*, *2*, 36-50, 2001.

Kain, J. S., and J. M. Fritsch, Convective parameterization for mesoscale models: The Kain-Fritsch scheme, The Representation of Cumulus Convection in Numerical Models, *Meteor. Monogr., No. 46*, Amer. Metero. Soc., 165-170, 1993.

Kiehl, J. T., and coauthors, The National Center for Atmospheric Research Community Climate Model: CCM3, *J. Climate, 11*, 1131-1149, 1998.

Klein, S. A., and C. Jakob, Validation and sensitivities of front clouds simulated by the ECMWF model. *Mon. Wea. Rev., 127*, 2514-2531, 1999.

Kuo, H. L., On formation and intensification of tropical cyclones through latent heat release by cumulus convection, *J. Atmos. Sci., 22*, 40-63, 1965.

Kuo, H. L., Further studies of the parameterization of the influence of cumulus convection on large-scale flow, *J. Atmos. Sci., 31*, 1232-1240, 1974.

Lin, W. Y., and M. H. Zhang, Evaluation of clouds and their radiation effects simulated by the NCAR Community Atmospheric Model CAM2 against satellite observations, *submitted to J. Climate, 2004.*

Minnis, P., W. L. Smith, D. P. Garber, J. K. Ayers, and D. R. Doeling, Cloud properties derived from GOES-7 for spring 1994 ARM Intensive Observing Period using version 1.0.0 of ARM satellite data analysis program. NASA Ref. Publ. 1366, 59pp., 1995. [Available from NASA Langley Research Center, Technical Library, MS 185, Hampton, VA 23655-5225]

Phillips, T. J., and coauthors, The CCPP-ARM Parameterization Testbed (CAPT): Where climate simulation meets weather prediction, *submitted to Bulletin of the AMS*, 2004.

Rogers, R., and J. M. Fritsch, A general framework for convective trigger functions, *Mon. Wea. Rev., 124*, 2438-2452, 1996.

Rossow, W. B., A. W. Walker, D. Beuschel, and M. Roiter, International Satellite Cloud Climatology Project (ISCCP) description of new cloud datasets. *WMO/TD, 737*, World Climate Research Programme (ICSU and WMO), 115 pp., 1996.

Stokes, G. M., and S. E. Schwartz, The Atmospheric Radiation Measurement (ARM) program: Programmatic background and design of the cloud and radiation test bed, *Bull. Amer. Meteor. Soc*., 75, 1202-1221, 1994.

Wang, J., and D. A. Randall, The moist available energy of a conditionally unstable atmosphere, II: Further analysis of the GATE data, *J. Atmos. Sci., 51*, 703-710, 1994.

Webb, M., C. Senior, S. Bony and J. J. Morcrette, Combining ERBE and ISCCP data to assess clouds in the Hadley Centre, ECMWF and LMD atmospheric climate models, *Climate Dynamics, 17*, 905-922, 2001.

Xie, S. C., Single-Column Modeling: Methodology and application to the evaluation of cumulus convection schemes in GCMs, Ph. D. thesis, *State University of New York at Stony Brook*, 126 PP., 1998.

Xie, S. C., and M. H. Zhang, Impact of the convective triggering function on single-column model simulations, *J. Geophys. Res., 105*, 14983-14996, 2000.

Xie, S. C., and coauthors, Intercomparison and evaluation of cumulus parameterizations under summertime midlatitude continental conditions, *Q. J. R. Meteorol. Soc., 128*, 1095-1135, 2002.

Zhang, G. J., and N. A. McFarlane, Convective Stabilization in Midlatitudes, *Mon. Weather Rev., 119*, 1915-1928, 1991.

Zhang, G. J., and N. A. McFarlane, Sensitivity of climate simulations to the parameterization of cumulus convection in the Canadian Climate Center general circulation model, *Atmosphere-Ocean, 33*, 407-446, 1995.

Zhang, G. J., Convective quasi-equalibrium in midlatitude continental environment and its effect on convective parameterization, *J. Geophys. Res., 107 (D14)*, 4220, doi:10.1029/2001JD001005, 2002.

Zhang, M. H., and J. L. Lin, Constrained variational analysis of sounding data bases on column-integrated budgets of mass, heat, moisture, and momentum: Approach and application to ARM measurements, *J. Atmos. Sci., 54*, 1503-1524, 1997.

Zhang, M. H., J. L. Lin, R. T. Cederwall, J. J. Yio, and S. C. Xie, Objective analysis of ARM IOP Data: Method and sensitivity, *Mon. Weather Rev., 129*, 295-311, 2001.

Figure Captions

Figure 1. (a) Relationship between CAPE (dotted) and surface precipitation in the ARM observations during the summer 1997 SGP IOP. (b) The observed (solid) and CCM3 SCM model-produced (dotted) surface precipitation rates (mm day^{-1}). (c) Relationship between DCAPE and surface precipitation in the ARM observations during the summer 1997 SGP IOP. (d) The observed (solid) and CCM3 SCM with an improved convective trigger produced (dotted) surface precipitation rates (mm day^{-1}).

Figure 2. The RMS errors (solid) in the ERA-40 reanalyses of (a) horizontal wind u-component, (b) v-component, (c) temperature, and (d) moisture during the ARM Summer 1997 IOP. Dashed lines represent standard deviations of the ARM observed fields.

Figure 3. The locations of the ARM five sounding balloons (✳), the seven NOAA wind profilers (◇), the CAM2 model grids (×), and the variational analysis domain (•) at the ARM SGP site. The letters A, B, C, and D represent the four CAM2 grid boxes centered by the model grid points (×), respectively.

Figure 4. The time series of the observed (solid) and model simulated (dotted) surface precipitation rates (mm day^{-1}) during the ARM 1997 Summer IOP. (a) CAM2O vs. OBS. (b) CAM2M vs. OBS.

Figure 5. The time series of the observed (solid) and model simulated (dotted) high clouds (%) during the ARM 1997 Summer IOP. (a) CAM2O vs. OBS. b) CAM2M vs. OBS.

Figure 6. The time series of the observed (solid) and model simulated (dotted) surface temperature (K) during the ARM 1997 Summer IOP. (a) CAM2O vs. OBS. (b) CAM2M vs. OBS.

Figure 7. The temporal evolution of (a) the ARM observed temperature, (b) differences between the CAM2O simulated temperature and the observations, and (c) differences between the CAM2M simulated temperature and the observations. The unit in the figure is K.

Figure 8. Same as Figure 7 except for the moisture field. The unit is g kg^{-1}.

Figure 9. Vertical profiles of a 30-day mean of 24-hour forecasts for (a) temperature errors (K) and (b) moisture errors (g kg^{-1}) produced by CAM2O (solid) and CAM2M (dash-dotted) over the ARM 1997 Summer IOP. The corresponding errors in the initial data are shown by the dotted lines in the figures.

Figure 10. Geographical distribution of a 30-day mean precipitation of 0-24 hour forecasts over the continental United States for (a) CAM2O, (b) CAM2M, and (c) the GPCP data, respectively.

Figure 11. Global distribution of a 30-day mean precipitation of 0-24 hour forecasts for (a) CAM2O, (b) CAM2M, and (c) the GPCP data, respectively.

Figure 12. Global distribution of a 30-day mean high clouds (daytime only) of 0-24 hour forecasts for (a) CAM2O, (b) CAM2M, and (c) the GPCP data, respectively.

Figure 13. Zonally averaged mean temperature over the 30 days from ERA-40 (a) and the differences between CAM2O and ERA-40 (b) and between CAM2M and ERA-40 (c). Unit is K. In (b) and (c), contour interval is 0.25. Contours larger than 0.5 or less than –0.5 are shaded. Solid lines are for contours greater than or equal to zero, and dotted lines for contours less than zero.

Figure 14. Zonally averaged mean moisture over the 30 days from ERA-40 (a) and the differences between CAM2O and ERA-40 (b) and between CAM2M and ERA-40 (c). Unit is g kg^{-1}. In (b) and (c), contour interval is 0.25. Contours larger than 0.5 or less than –0.5 are

shaded. Solid lines are for contours greater than or equal to zero, and dotted lines for contours less than zero.

Figure 15. Zonally averaged mean zonal wind over the 30 days from ERA-40 (a) and the differences between CAM2O and ERA-40 (b) and between CAM2M and ERA-40 (c). Unit is m s^{-1}. In (b) and (c), contour interval is 0.5. Contours larger than 0.5 or less than –0.5 are shaded. Solid lines are for contours greater than or equal to zero, and dotted lines for contours less than zero.

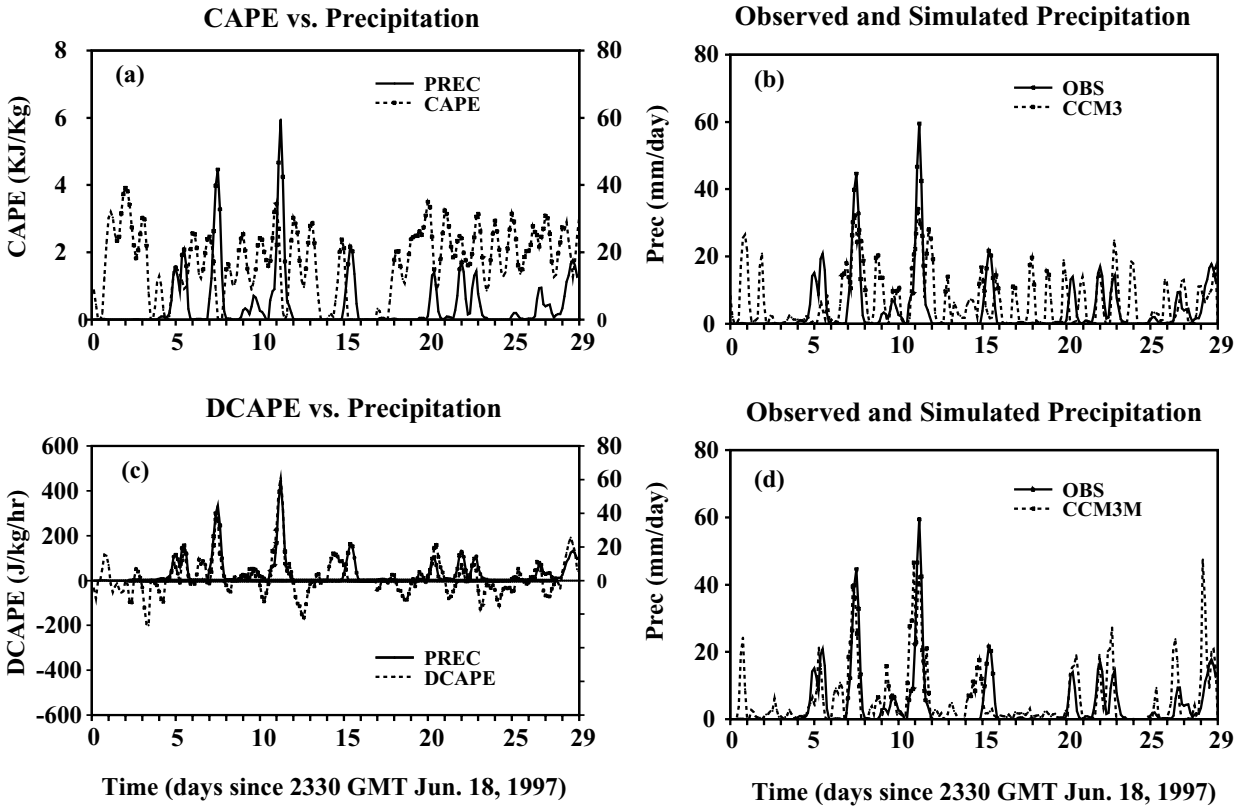

Figure 1. (a) Relationship between CAPE (dotted) and surface precipitation in the ARM observations during the summer 1997 SGP IOP. (b) The observed (solid) and CCM3 SCM model-produced (dotted) surface precipitation rates (mm day^{-1}). (c) Relationship between DCAPE and surface precipitation in the ARM observations during the summer 1997 SGP IOP. (d) The observed (solid) and CCM3 SCM with an improved convective trigger produced (dotted) surface precipitation rates (mm day^{-1}).

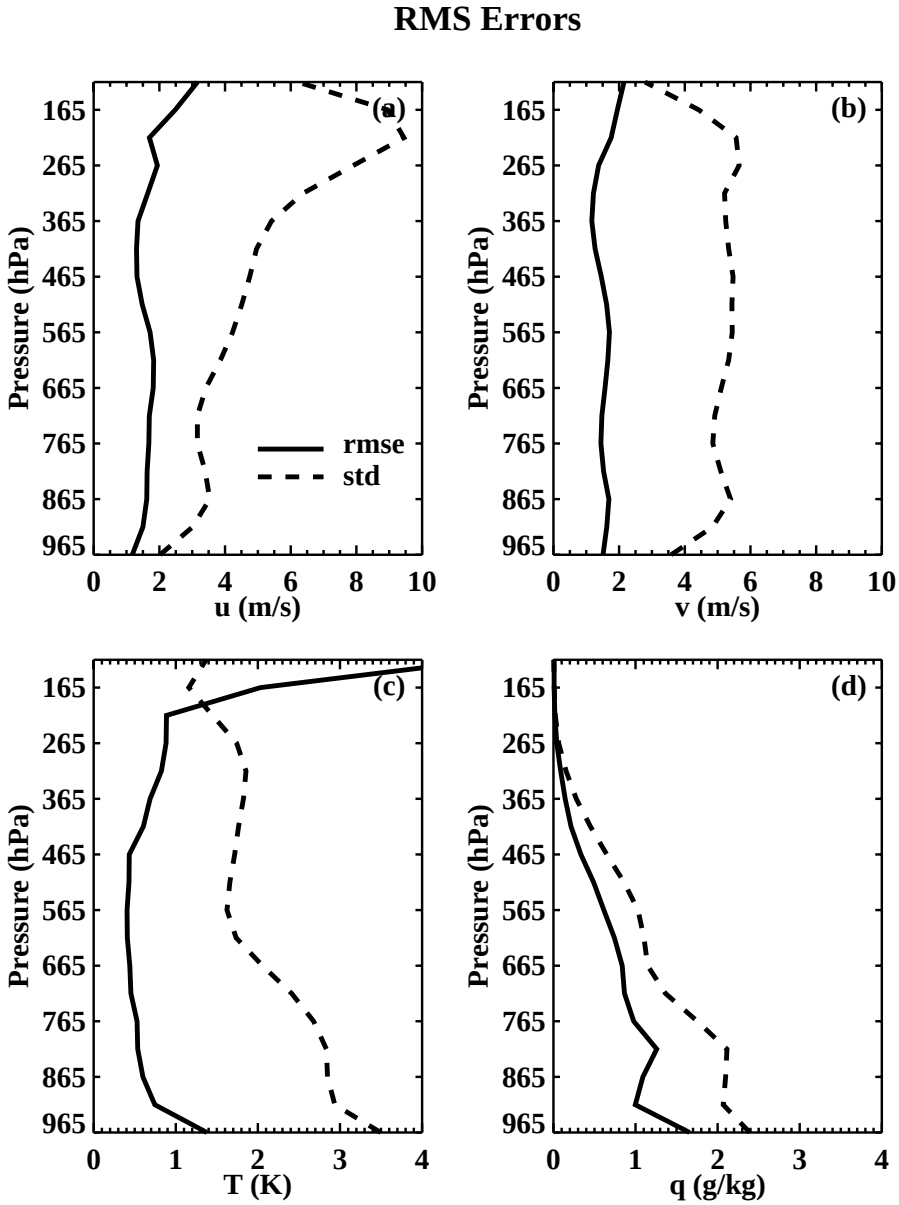

Figure 2. The RMS errors (solid) in the ERA-40 reanalyses of (a) horizontal wind u-component, (b) v-component, (c) temperature, and (d) moisture during the ARM Summer 1997 IOP. Dashed lines represent standard deviations of the ARM observed fields.

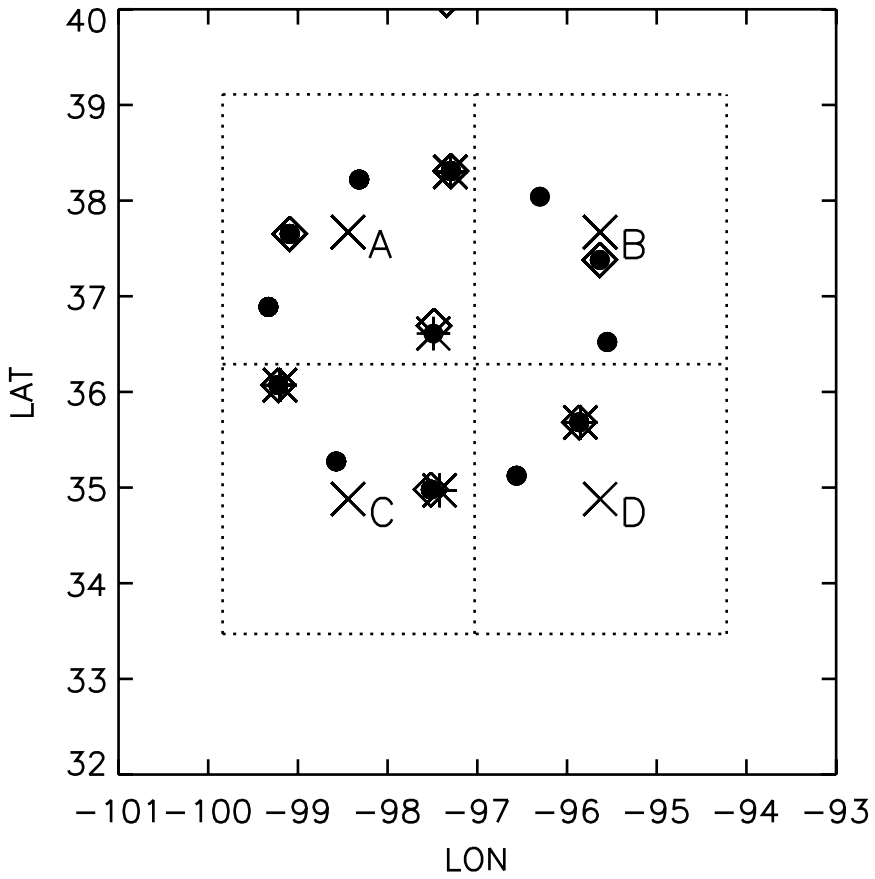

Figure 3. The locations of the ARM five sounding balloons (✳), the seven NOAA wind profilers (◇), the CAM2 model grids (×), and the variational analysis domain (•) at the ARM SGP site. The letters A, B, C, and D represent the four CAM2 grid boxes centered by the model grid points (×), respectively.

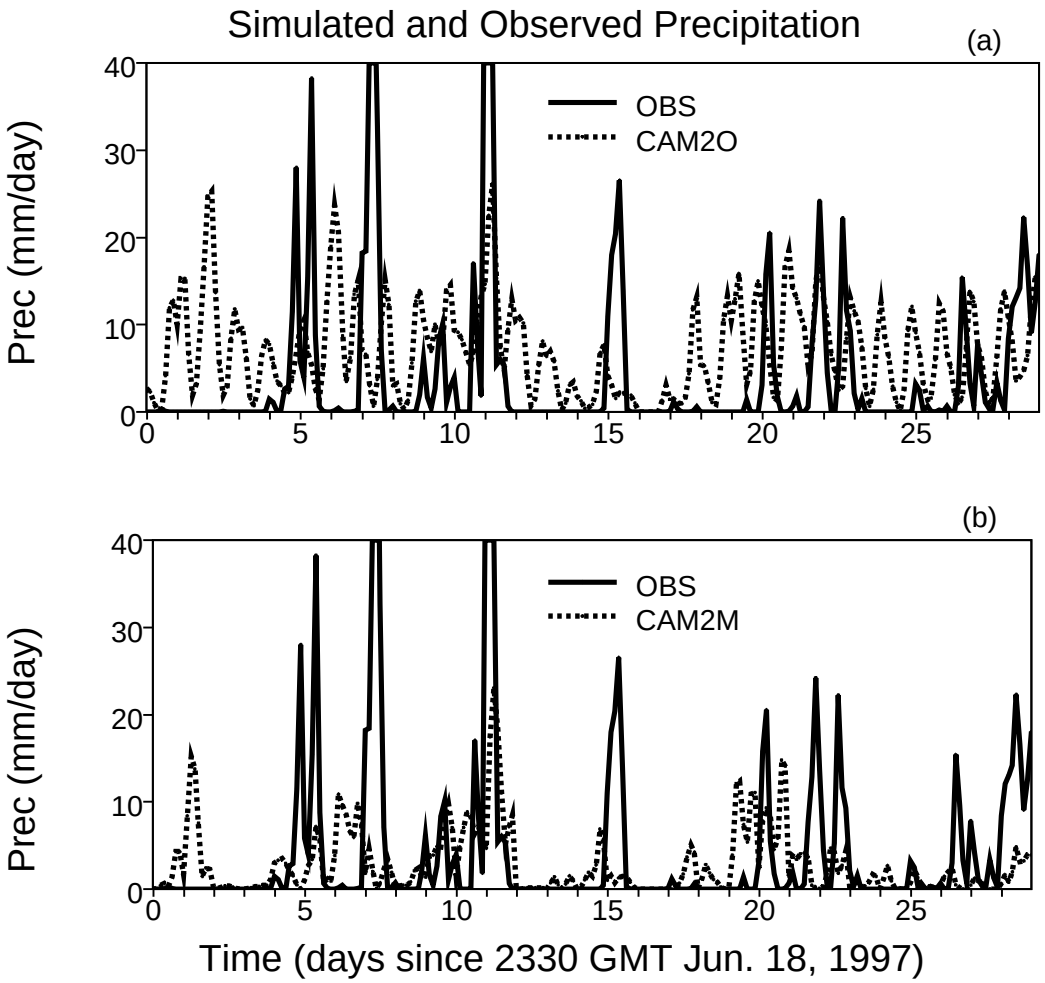

Figure 4. The time series of the observed (solid) and model simulated (dotted) surface precipitation rates (mm day^{-1}) during the ARM 1997 Summer IOP. (a) CAM2O vs. OBS. (b) CAM2M vs. OBS.

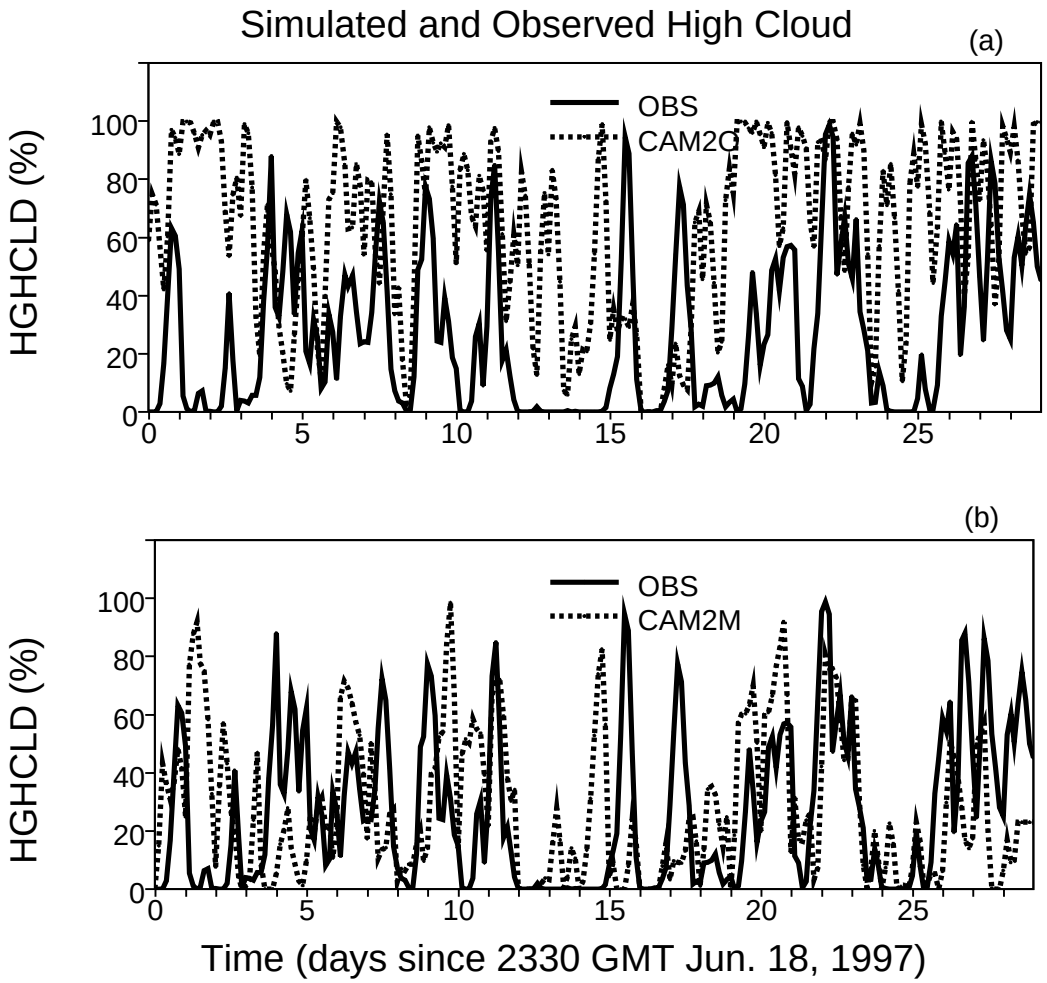

Figure 5. The time series of the observed (solid) and model simulated (dotted) high clouds (%) during the ARM 1997 Summer IOP. (a) CAM2O vs. OBS. (b) CAM2M vs. OBS.

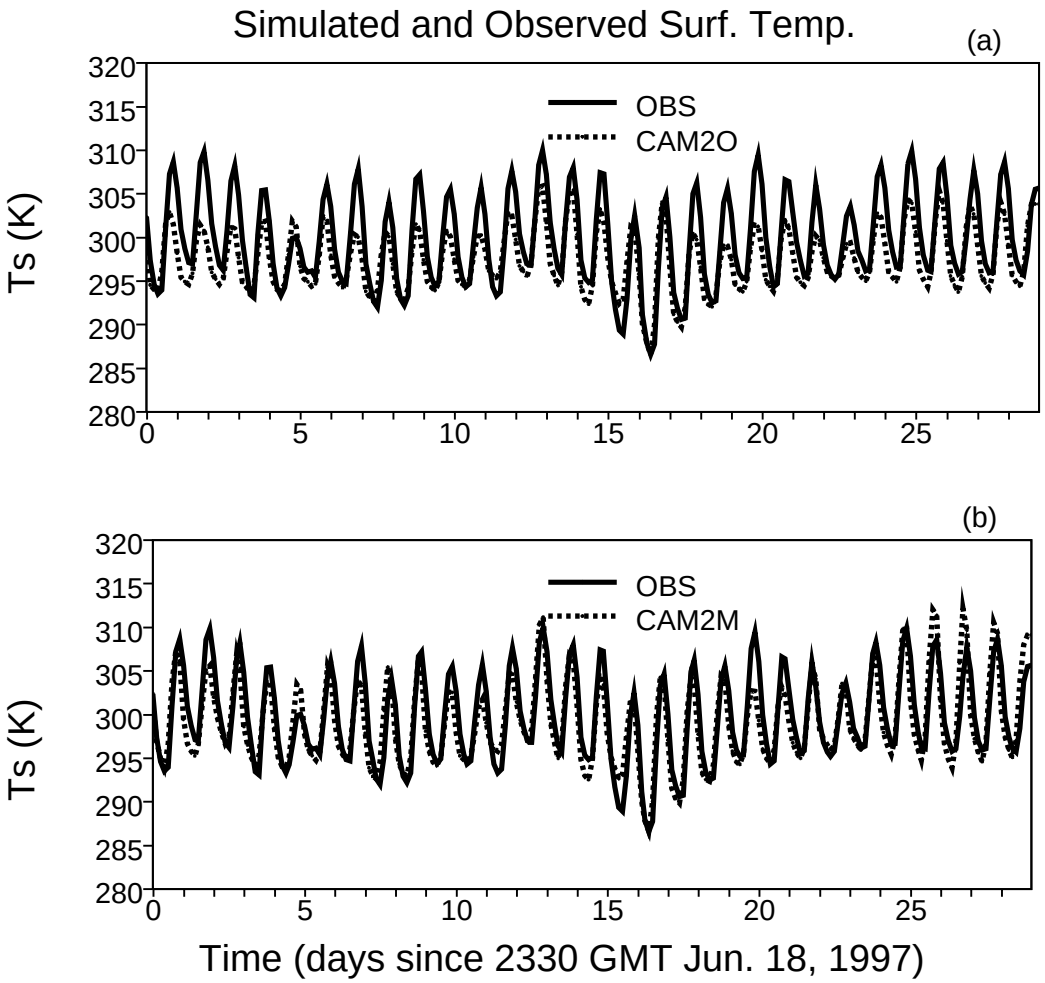

Figure 6. The time series of the observed (solid) and model simulated (dotted) surface temperature (K) during the ARM 1997 Summer IOP. (a) CAM2O vs. OBS. (b) CAM2M vs. OBS.

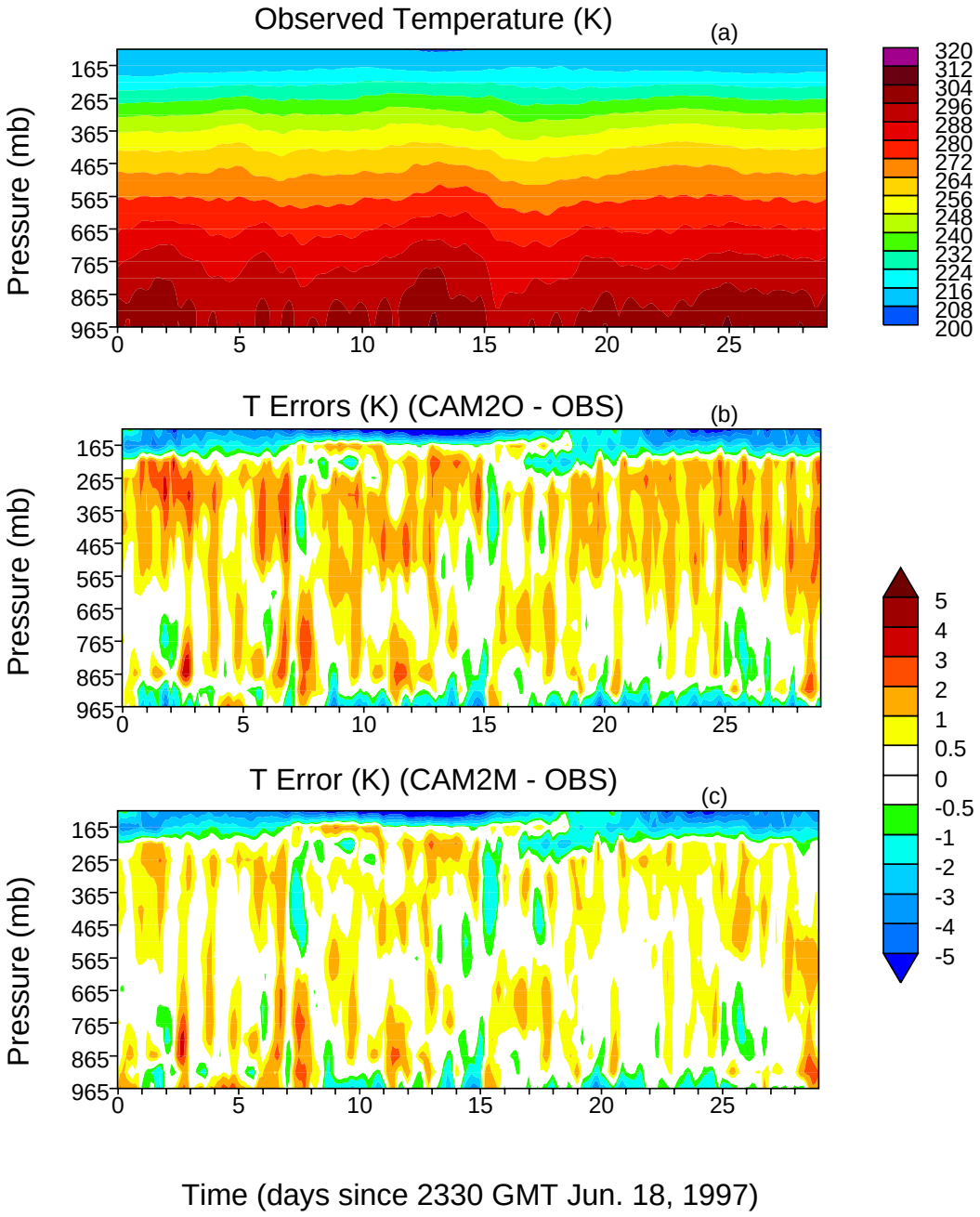

Figure 7. The temporal evolution of (a) the ARM observed temperature, (b) differences between the CAM2O simulated temperature and the observations, and (c) differences between the CAM2M simulated temperature and the observations. The unit in the figure is K.

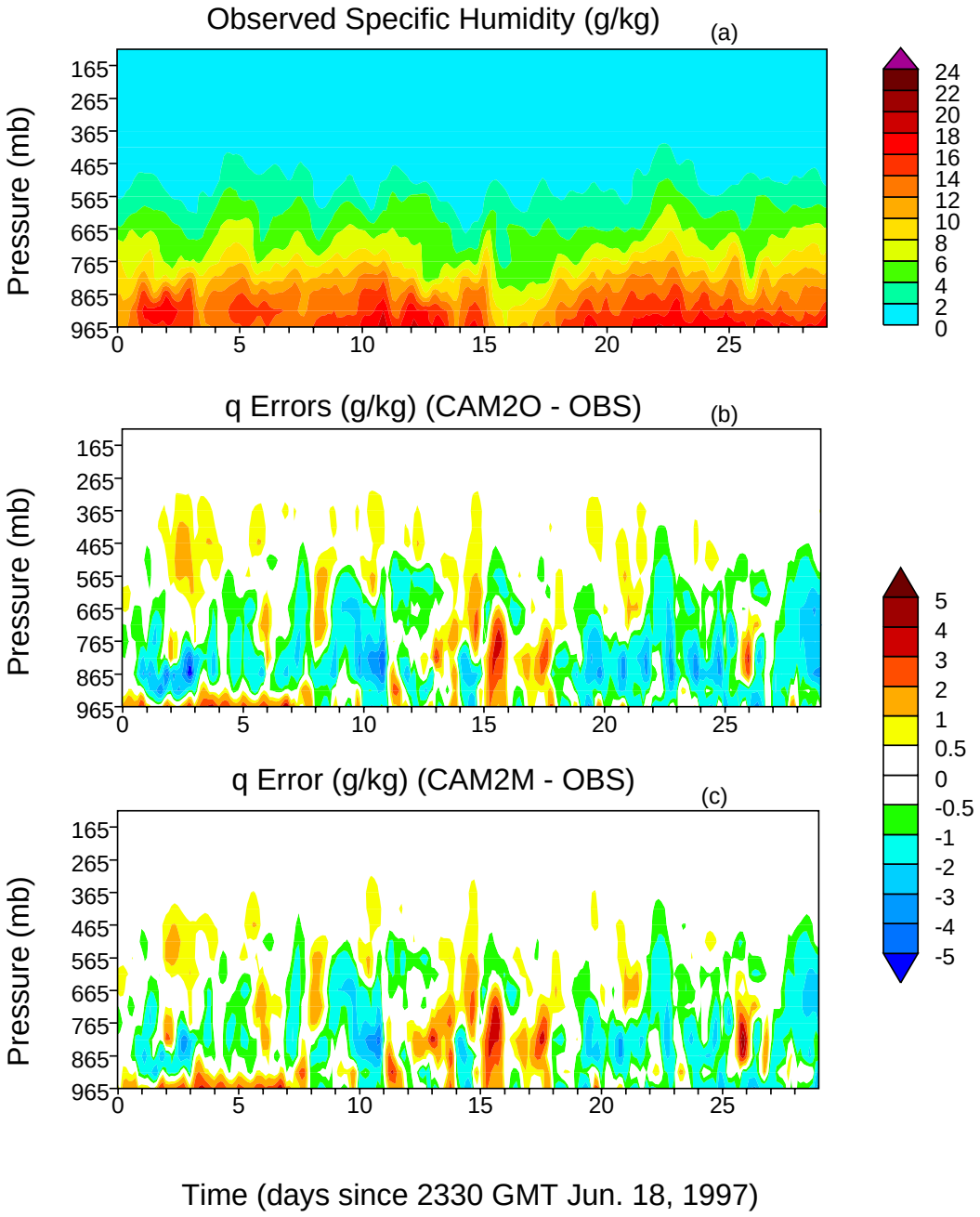

Figure 8. Same as Figure 7 except for the moisture field. The unit is g kg^{-1}.

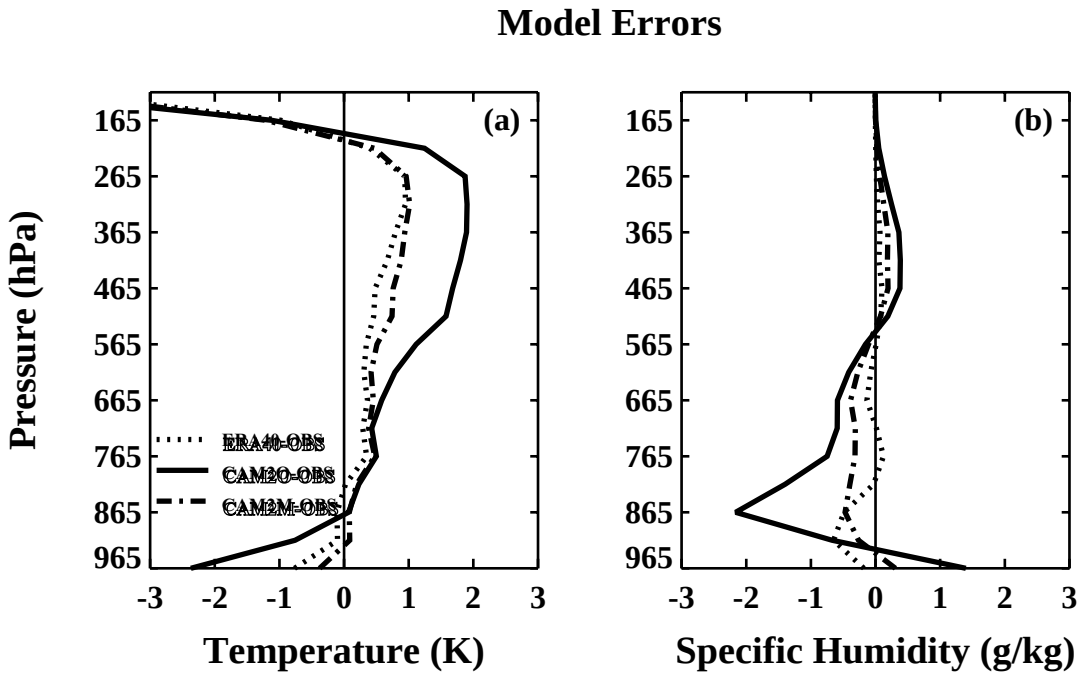

Figure 9. Vertical profiles of a 30-day mean of 24 hour forecasts for (a) temperature errors (K) and (b) moisture errors (g kg^{-1}) produced by CAM2O (solid) and CAM2M (dash-dotted) over the ARM 1997 Summer IOP. The corresponding errors in the initial data are shown by the dotted lines in the figures.

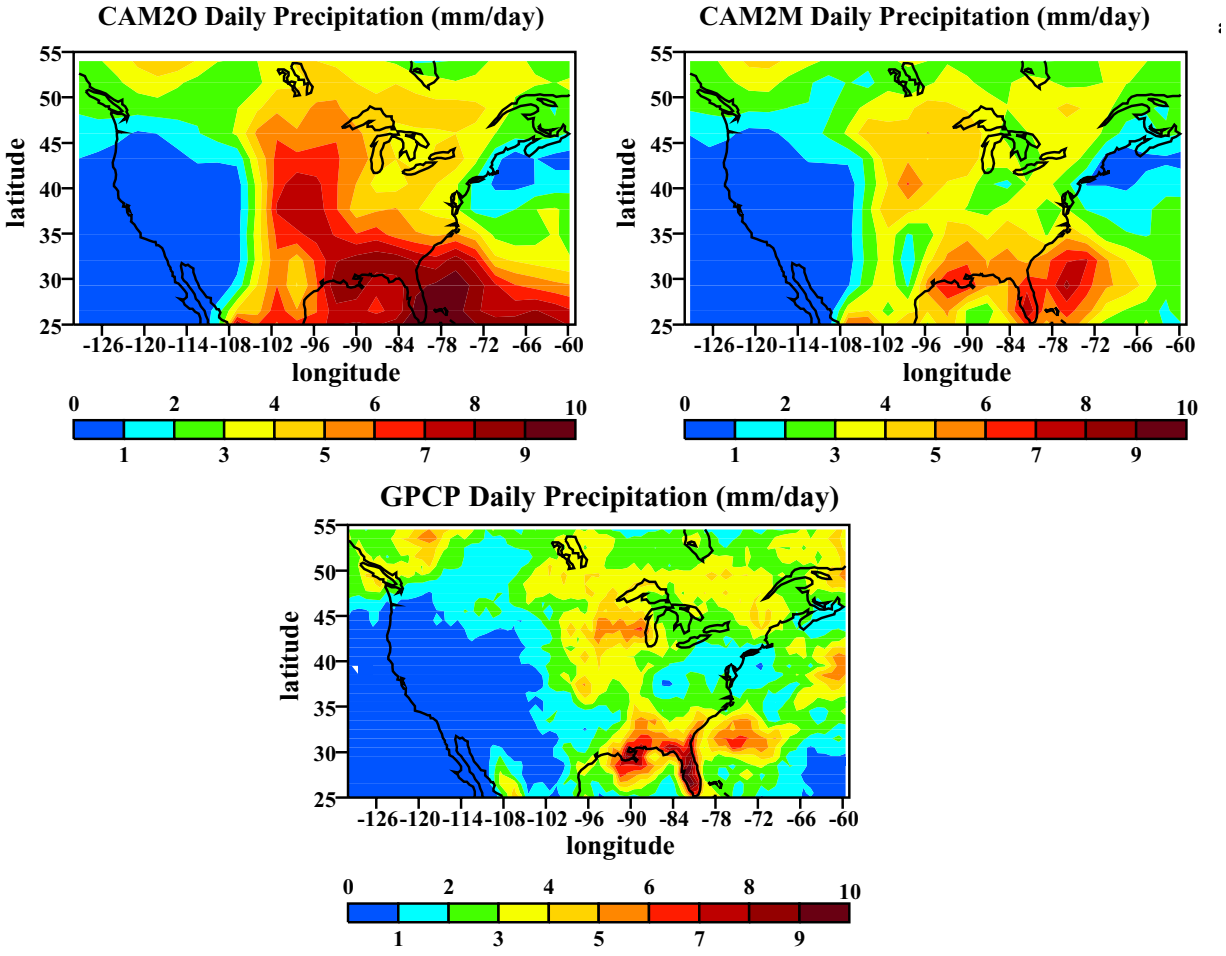

Figure 10. Geographical distribution of a 30-day mean precipitation of 0-24 hour forecasts over the continental United States for (a) CAM2O, (b) CAM2M, and (c) the GPCP data, respectively.

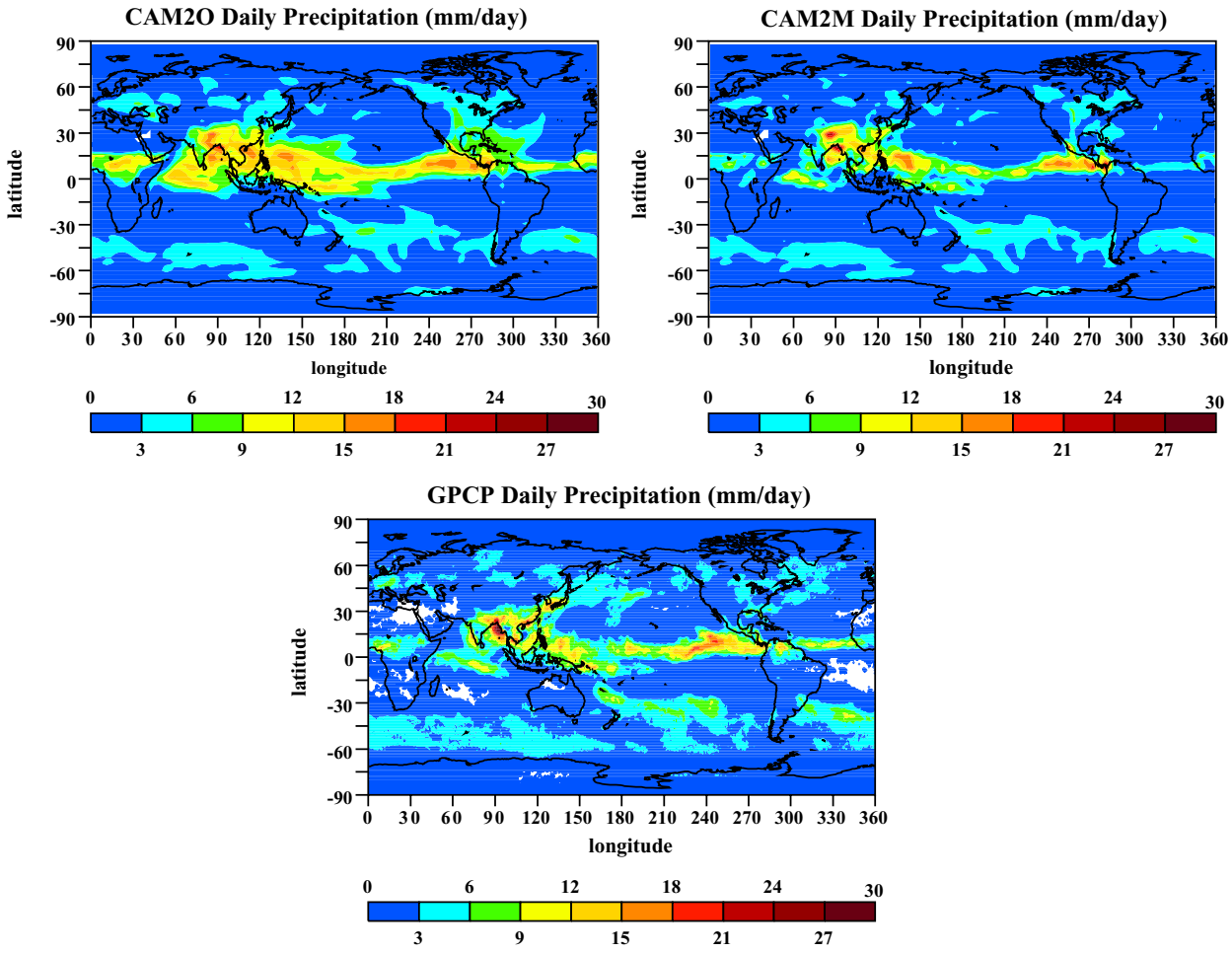

Figure 11. Global distribution of a 30-day mean precipitation of 0-24 hour forecasts for (a) CAM2O, (b) CAM2M, and (c) the GPCP data, respectively.

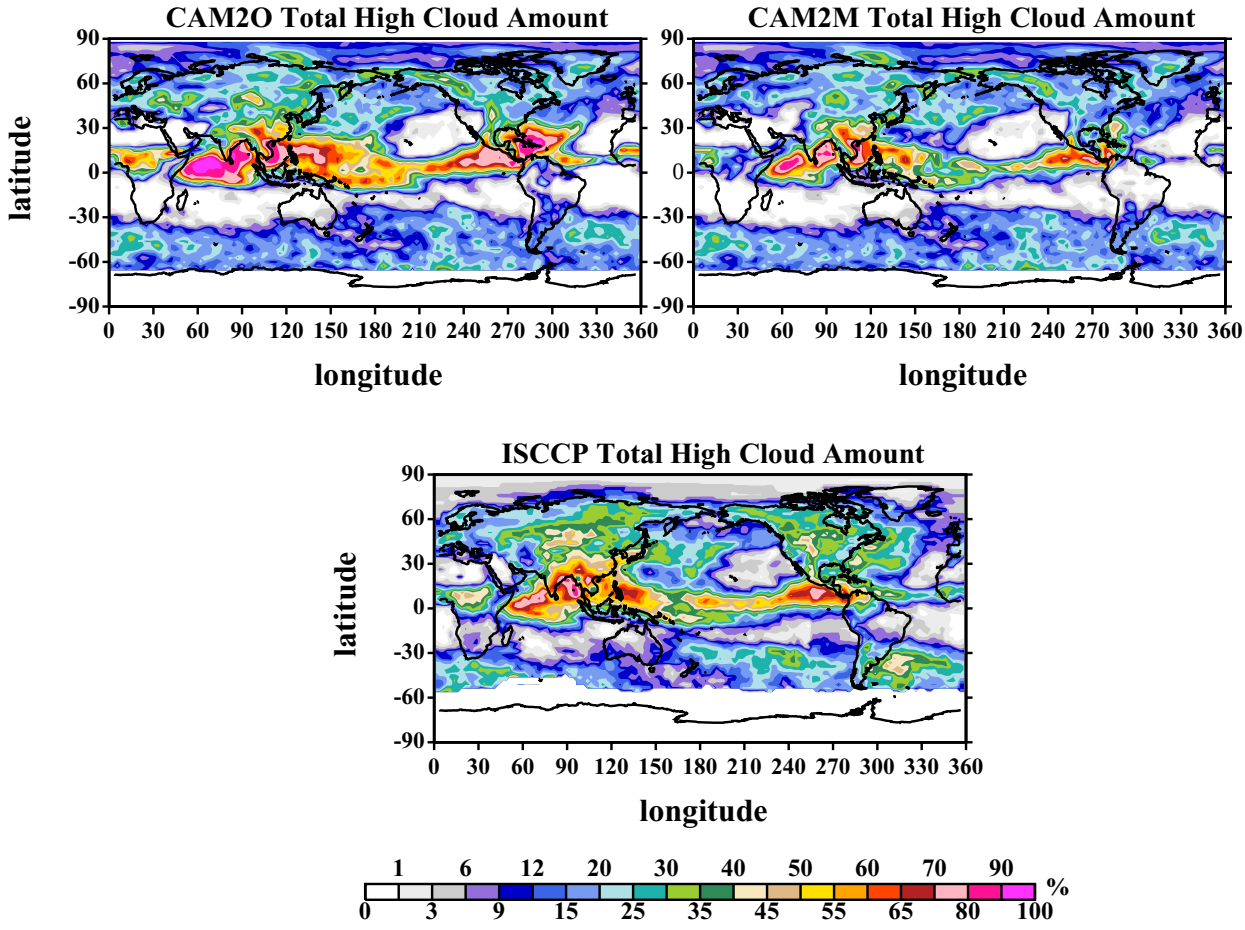

Figure 12. Global distribution of a 30-day mean high clouds (daytime only) of 0-24 hour forecasts for (a) CAM2O, (b) CAM2M, and (c) the GPCP data, respectively.

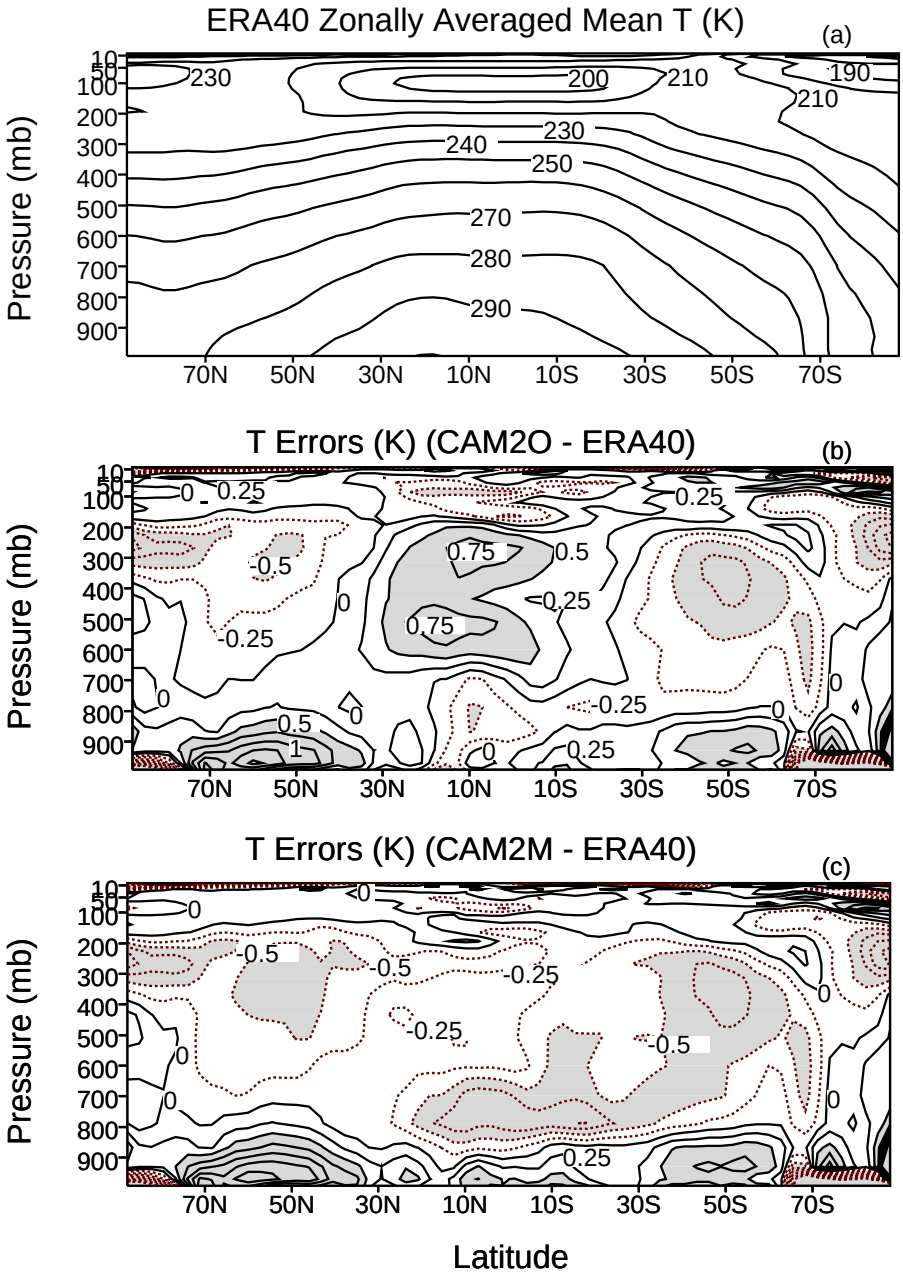

Figure 13. Zonally averaged mean temperature over the 30 days from ERA-40 (a) and the differences between CAM2O and ERA-40 (b) and between CAM2M and ERA-40 (c). Unit is K. In (b) and (c), contour interval is 0.25. Contours larger than 0.5 or less than –0.5 are shaded. Solid lines are for contours greater than or equal to zero, and dotted lines for contours less than zero.

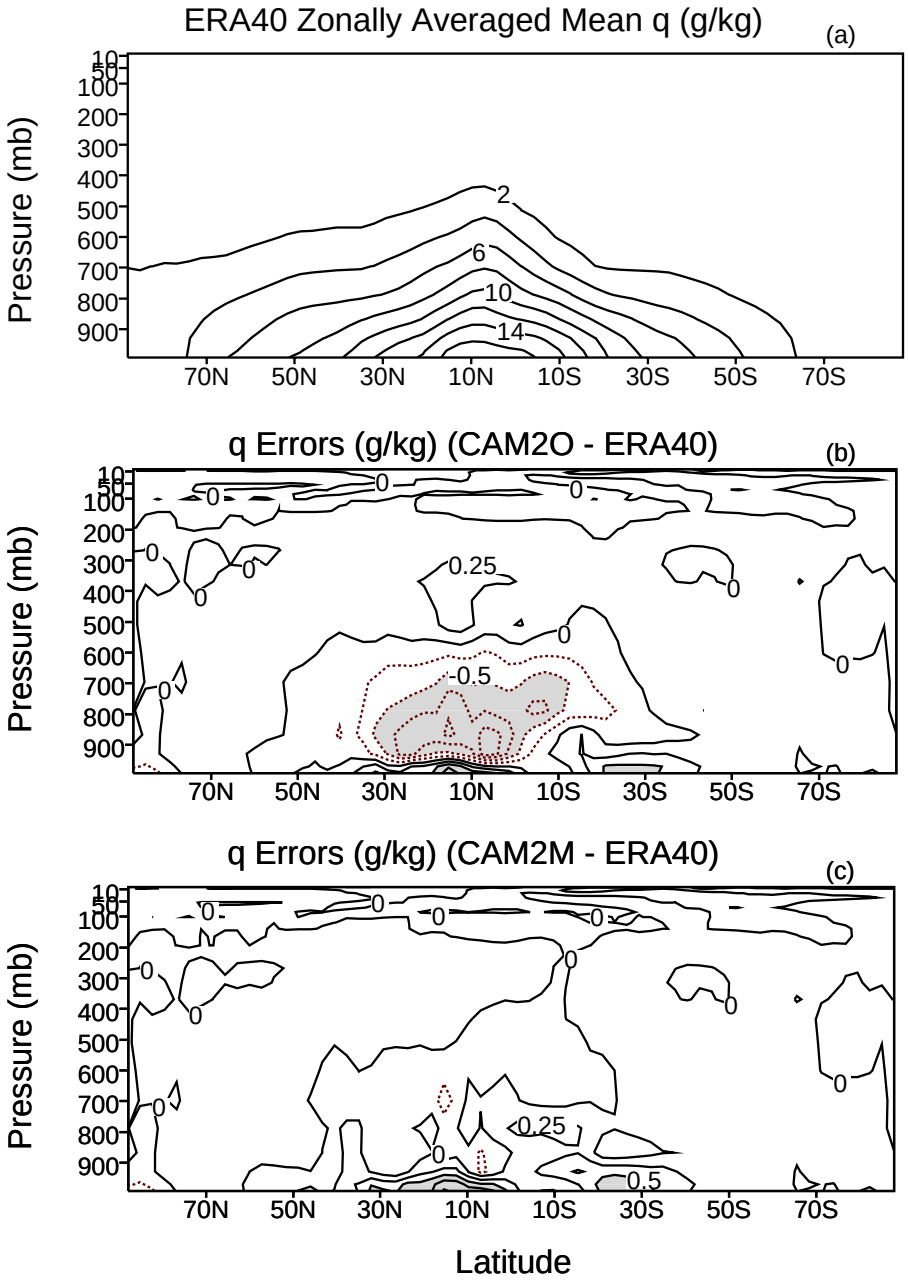

Figure 14. Zonally averaged mean moisture over the 30 days from ERA-40 (a) and the differences between CAM2O and ERA-40 (b) and between CAM2M and ERA-40 (c). Unit is g kg^{-1}. In (b) and (c), contour interval is 0.25. Contours larger than 0.5 or less than –0.5 are shaded. Solid lines are for contours greater than or equal to zero, and dotted lines for contours less than zero.

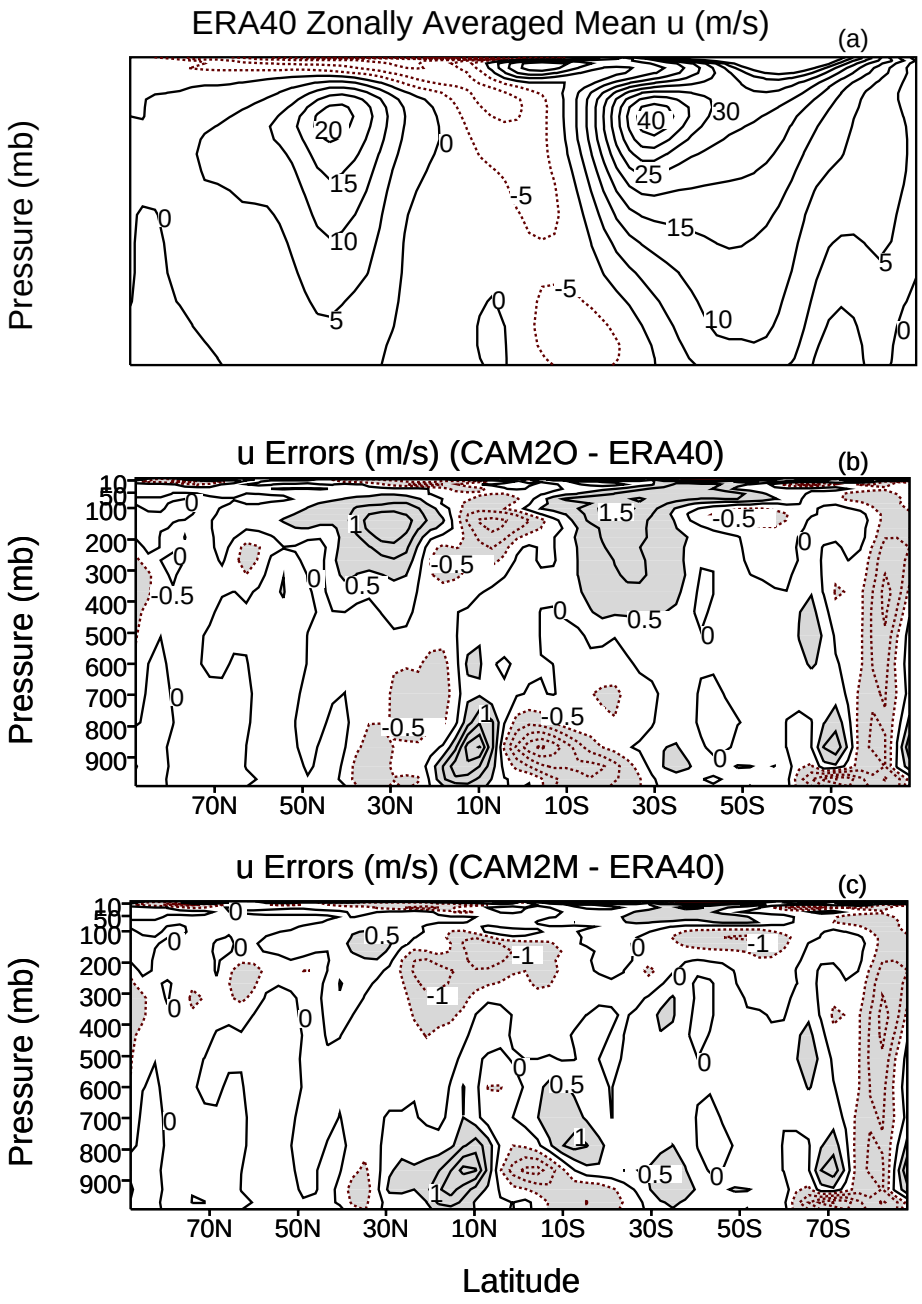

Figure 15. Zonally averaged mean zonal wind over the 30 days from ERA-40 (a) and the differences between CAM2O and ERA-40 (b) and between CAM2M and ERA-40 (c). Unit is m s^{-1}. In (b) and (c), contour interval is 0.5. Contours larger than 0.5 or less than –0.5 are shaded. Solid lines are for contours greater than or equal to zero, and dotted lines for contours less than zero.